DOI: 10.1002/ ((please add manuscript number))
Article type: Full Paper

Ergodic light propagation in a half-cylinder photonic plate for optimal absorption in perovskite solar cells

Guillermo Martínez-Denegri, Silvia Colodrero, Quan Liu, Johann Toudert, Gregory Kozyreff, and Jordi Martorell**

G. Martínez-Denegri, Dr. S. Colodrero, Dr. Q. Liu, Dr. J. Toudert, Prof. J. Martorell
ICFO-Institut de Ciencies Fotoniques, The Barcelona Institute of Science and Technology, 08860 Castelldefels, Spain.
E-mail: jordi.martorell@icfo.eu
E-mail: guillermo.martinez-denegri@icfo.eu

Prof. J. Martorell
Departament de Física, Universitat Politecnica de Catalunya, Terrassa 08222, Spain.

Prof. G. Kozyreff
Optique Nonlinéaire Théorique, Université libre de Bruxelles (U.L.B.), Campus de la Plaine CP 231, B-1050 Bruxelles, Belgium.

KEYWORDS: Ergodic, light trapping, perovskite solar cells, periodicity, photonic plate

In an optical medium slab a randomization of the interfaces would lead to an ergodic light propagation implying a kind of light trapping that sets an upper limit for a broadband absorption enhancement factor. However, in thin film solar cells where such light trapping is most needed, it is not straightforward how the implementation of a surface randomization should be done. In addition, such randomization may also severely limit the electronic device performance. In here, we introduce a cylindrical periodic corrugation, which we named half-cylinder photonic plate, at the light entering interface which leads to an ergodic light propagation. We take advantage of such ergodicity to enhance light absorption in a perovskite cell physically separated by a planar glass substrate from such half-cylinder photonic plate. Theoretically and experimentally we demonstrate that the enhancement light absorption factor we measured is close to the maximum possible for light trapping schemes using one interface periodic corrugations. This upper limit results from the ergodic light propagation we achieve with a half-cylinder photonic plate made from an optical transparent material with a low refractive index that minimizes light rejection by reflectivity.

1. Introduction

In an ergodic optical medium the light intensity can be up to n^2 times the incident light intensity, being *n* the local index of refraction, or two times that if a diffusive reflective surface is placed behind. If the surface of such optical medium is quite irregular in shape any incident ray upon entering the medium will lose memory of the external incident state, defined by the angle of incidence relative to the local surface normal, after one or two scattering events.[1] In that case, a collimated incident beam will produce a random distribution of light and the n^2 enhancement will be achieved provided that the light rays internal to the medium behave ergodically. To reach such kind of wavelength independent light trapping is of fundamental interest in solar cells, which performance relies on an effective broadband light absorption.[2–4] Unfortunately, except in rare cases where the surface random texturing is inherent to the cell structure,[5–7] introducing such disorder may have a negative effect on the electrical performance of the solar cell device. In a recent work it was noted that a randomly textured surface is not strictly necessary to achieve ergodicity.[8] Indeed, a periodically corrugated optical medium composed of intercalated optical fibers forming a plate, named photonic fiber plate (PFP), was shown to lead to a chaotic light ray propagation that was used to enhance light absorption from an evaporated organic solar cell fabricated on one side of such PFP. Although the regularity of the periodic surface certainly simplified the thin film solar device fabrication, it limited layer deposition to processes fully based on high vacuum evaporation or sputtering.

Herein, we combine the periodically corrugated surface from the PFP on one side of an optical layered medium with a planar interface on the opposite side where a high performance solution processed perovskite solar cell can be fabricated. The strategy followed for the fabrication of the solar cells consisted on combining two different reported methods[9,10] in

order to achieve highly efficient devices using low temperature processes. The top interface of the layered medium is formed by a periodic array of half cylinders, which we name half-cylinder photonic plate (h-CPP). As it will be seen below, thanks to the large thickness of the optical medium that separates the h-CPP top surface from the bottom flat interface where the cell is located, after a first bounce on the bottom interface a nearly random incident angle is achieved for the non-absorbed light rays when reaching to the top interface. It can be estimated that 97% of the incident light rays that fall on a given cylinder are directed to another cylinder upon the first bounce on the bottom of the optical medium. In contrast to other recent approaches to enhance light absorption in perovskite solar cells[11–15] where an angular randomization leading to an ergodic optical geometry was not confirmed, we demonstrate that the short circuit current enhancement we achieved is very close the maximum possible and it can be qualitatively and quantitatively predicted by a model that combines ray and wave optics which establishes the ergodicity of the h-CPP structure considered.

2. Theoretical Model

As the geometrical dimensions of the h-CPP are large compared to the wavelengths of interest, a ray picture is suitable to describe light trapping. Examination of **Figure 1**a indicates that ray trajectories depend sensitively on the initial conditions, which is on where the ray is incident on the h-CPP. Between two refraction/reflection events, the photons follow a ballistic trajectory. Therefore the ray paths are entirely encoded in the set incidence angle β_j that the j^{th} segment of ray makes with the interface at which it refracts or reflects. To confirm from a geometrical optics perspective the ergodic character of the h-CPP geometry, one must determine the fraction of incoming rays which will follow an unpredictable trajectory upon entering the h-CPP. Indeed, any ray travelling to a different cylinder from its original one will

subsequently undergo reflection/refraction with practically unpredictable angle. Such fraction is given by

$$f = 1 - \frac{2x}{p} \quad (1)$$

where, as shown in the inset of Figure 1b, x corresponds to the smallest horizontal distance between the top of a given cylinder and a ray that upon a reflection at the bottom interface enters a neighbouring cylinder of the array, while p is the period of the h-CPP. Provided x is small compared to p, it is straightforward to show that the fraction of incident rays that upon incidence will follow a quasi unpredictable trajectory is:

$$f \approx 1 - \frac{nd}{4h} \quad (2)$$

where h is the separation between the corrugated and planar interfaces of the h-CPP, n its index of refraction and d the diameter of the cylinder. When n = 1.45, d = 104 μm, and h=1.15 mm, one obtains that such fraction is 97%.

In order to characterize the ray dynamics from a statistical point of view, it appears useful to monitor not β_j but $\Delta\beta_j = \beta_j - \beta_{j-1}$. Indeed, rays bouncing on a circular boundary, and thus temporarily following a regular trajectory, satisfy $\Delta\beta_j=0$. In Figure 1b, we plot the Cumulative Distribution Function (CDF) of Δβ, which is the integral of the probability distribution of Δβ. The CDF is computed as in Ref. 8 by a ray tracing algorithm that generates a large sample of ray segments in the h-CPP, consecutively to a single ray impinging on the device. We keep track of ray trajectories until the ray intensities have a very small value (0.0001 times its original value) in order to generate a sufficiently large statistical sample. We observe that we converge to the same CDF independently on the initial condition, i.e. where the initial ray fell on the device and its incidence angle. In all our simulations we considered both parallel and perpendicular polarizations to the cylinder axes and took the average. Only a small difference was observed between the two polarizations, which we mainly attribute to the Fresnel coefficients at the air/h-CPP interface. We note that the CDF undergoes a finite jump at Δβ=0.

This indicates that a sizeable, finite probability is associated to that value. Hence, even though the ray trajectory is chaotic, a fraction of it is regular. This demonstrates that the ray chaos achieved by the h-CPP is of the intermittent type. In addition, we note that the CDF, computed from a large set of numerically computed segments of ray, does not depend on the initial condition of the simulations. Hence, independently on the initial conditions, any region of the phase space of the ray trajectories can be visited. This constitutes a numerical proof of ray ergodicity. Note that ergodicity is understood here in relation to the geometrical redistribution of the rays segments inside the h-CPP and independently on their intensity, as in Ref. 1. The absorption of the intensity brought in by a particular incoming ray does, of course, depend on its initial conditions, as described in Ref. 8.

When a solar cell is incorporated on the side of the substrate opposite to the h-CPP, to take full advantage of the ergodic ray propagation, the refractive indexes of all layers, from the h-CPP to the active cell layer, should, in principle, be matched. However, increasing the refractive index of the h-CPP/substrate towards the higher index the active layer would lead to an increased reflectivity at the air/h-CPP interface. Using a numerical approach that combines ray optics propagation in the h-CPP/substrate structure with wave propagation in the multilayer cell structure, one can numerically compute, for different values of the index of the h-CPP/substrate, the external quantum efficiencies (EQEs) and corresponding short circuit currents. When a perovskite cell is considered, both magnitudes are shown as a function of the light incident wavelength in **Figure S1** and **Figure S2** of the Supporting Information, respectively. As can be seen in Figure 1c, an optimal light absorption is obtained when the index of refraction of the h-CPP/substrate structure is in the 1.4-1.65 range. In other words, a maximum absorption is obtained when the adequate balance between minimizing reflectivity at the air/h-CPP interface and matching the indexes of the substrate and cell structure is reached. Provided the h-CPP structure exhibits a 96% randomization capacity, we may conclude that any other kind of regular or periodic[11,16,17] interface structuration would yield,

at best, the same enhancement achieved by the h-CPP. Rather than a different kind of interface structuration, a further enhancement of the light absorption percentage would require, either a better back mirror to reduce parasite absorption or, a thinner active layer as shown in **Figure S3** of the Supporting Information. It is worth noting that for the h-CPP configuration and a 300 nm thick active layer, the short circuit current approaches the one obtained from a 600 nm thick active layer in the standard planar configuration.

3. Experimental Results

The light trapping and harvesting configuration considered consists of an h-CPP deposited on one side of a 1 mm thick fused quartz glass substrate and a perovskite solar cell deposited on the opposite side of that same substrate. The overall structure and the method to fabricate it we implemented allow to integrate a light trapping element with a solar cell without having to impose any restrictions or limitations on the fabrication of the solar device. As indicated above we implemented such light trapping structure for perovskite solar cells provided light absorption is never complete for the standard perovskite cell configuration,[18,19] especially in the near IR region of the sun spectrum which is, in principle, the most interesting because it exhibits the largest photon flux.

The solar cell structure employed for this study, which SEM cross section is shown in **Figure 2**a, was ITO (100nm)/SnO_2 (20 nm)/$(FAI)_x(MABr)_{1-x}PbI_2$ (600 nm)/Spiro (200 nm)/Au (60 nm). This cell was fabricated following a low temperature process as described in the Materials and Methods section. As schematically shown in **Scheme 1**, an h-CPP of PDMS was fabricated separately and subsequently deposited on the unused side of the glass substrate. We used PDMS because its index of refraction falls within the index range for maximum light absorption enhancement as can be seen in Figure 1c. Additionally, PDMS is a highly transparent optical material which can be molded and cured easily. First, a PDMS layer was deposited by spin-coating on top of a 1”x1” aluminum-nickel master patterned with the

negative h-CPP structure (Film Optics Ltd.). Then, the PDMS was cured at 90 ºC during one hour and removed from the master obtaining a flexible free standing h-CPP, shown in Figure 2b, consisting of 110 intersected semi-cylinders per cm with 104 μm in diameter, being their centers separated by 91 μm. The 1"x1" h-CPP obtained was deposited by simple physical contact on the bare glass substrate side opposite to the side were the perovskite cell was previously grown.

To determine the effect of the h-CPP on the perovskite solar cell performance we measured the J-V curve and determined the corresponding photovoltaic parameters. Provided that the h-CPP can be easily deposited and removed from the glass substrate without affecting the photovoltaic device operation, to analyze the h-CPP's contribution on the cell performance in a reliable manner, the photovoltaic parameters of the same exact solar cell were measured with and without the h-CPP. In **Figure 3**a one may observe how the Jsc of the perovskite solar cell is enhanced from 22 mA/cm^2 to 22.57 mA/cm^2 when the h-CPP is applied on it. As expected, the rest of PV parameters, Voc and FF, were essentially not affected when the h-CPP was applied on the solar cell. In other words, the increase of the photocurrent is the main factor that causes a PCE increase from 18.10 % to 18.77% for the cell which J-V curve is shown in Figure 3a. In total, 24 devices were analyzed and their box plot diagrams for the corresponding PV parameters shown in Figures 3b-e. Herein, it is confirmed that, essentially, the only parameters modified by the application of the h-CPP were the Jsc and, consequently, the PCE, whilst the Voc and the FF remained almost unaltered. From Table 1, one may note that the average gain on Jsc brought by the h-CPP was 0.58 mA/cm^2 corresponding to a 2.7% photocurrent enhancement, which led to a maximum PCE of 19.8% for the cells incorporating the h-CPP.

4. Discussion

The PV parameter study above confirms that the use of the h-CPP in perovskite solar cells leads to an overall enhancement in light absorption and cell performance. To gain further insight into such enhancement, we computed the EQE for perovskite solar cells with and without the h-CPP and then compared them to the experimentally measured ones. From the numerically computed EQEs shown in **Figure 4**a, one may clearly distinguish two very distinct features. On the one hand, the h-CPP structure contributes to an enhanced absorption in spectral regions where the absorption coefficient of the perovskite is weaker, such as for instance in the near infrared where a clear enhancement, peaking at the perovskite absorption edge, is seen in Figure 4a. On the other hand, the h-CPP structure has a tendency to flatten the EQE, pushing such EQE close to the corresponding IQE, by compensating for the destructive interference between the forward and backward propagating light waves. Valleys in the EQE of the cell without h-CPP, which are distinguishable at around 500 nm and 725 nm, are likely to be the result of such destructive interference provided they do not match to any decrease in the perovskite extinction coefficient shown in **Figure S4** of the supporting information. The destructive interference is a consequence of the multilayer dielectric structure inherent to any photovoltaic thin film device.[20,21] In both cases, weak absorption or destructive interference, the ergodic light propagation brought by the h-CPP structure has the effect to effectively increase the length for the light path in the perovskite layer. The main features observed in the numerically computed EQE enhancement curve are to a large extent reproduced in the experimentally determined one shown in Figure 4b. Indeed, the peak of the enhancement curve at the absorption edge and the tendency to broadly flatten the EQE are also confirmed experimentally. Nonetheless, one should not expect a perfect matching between theory and experiment provided large variations are observed in the complex refractive indexes of different perovskite layers caused by uncontrollable alterations in the growth procedure of such layers.

5. Conclusions

To conclude we have demonstrated that a simple ordered cylindrical structuration of the photovoltaic device interface that separates the transparent substrate from the outside can lead to a chaotic light propagation and a full randomization of the light propagation. We have also demonstrated that it is possible to obtain such periodic structuration on a large area using a simple procedure based on the spin coating of PDMS on a negative template and then, by a simple deposition on a flat glass surface of the structured PDMS layer mechanically separated from the template, fabricate a photovoltaic device capable to trap light effectively. In the solar devices that we fabricated and characterized, we confirmed that the short circuit current enhancement we achieved was accurately predicted by a ray optic model which established ergodicity in the light propagation in the h-CPP structure. Using the same ray optics approach combined with a transfer matrix based computation of light absorption in the active layer of the cell, we estimated the EQE, and confirmed that the predicted gain in EQE agrees with the experimentally measured one. Although the increase in performance is limited when a reference cell with an already high PCE is used, it is close to the maximum achievable for any kind of regular or periodic structuration at the light entering interface. The h-CPP proposed may find an interesting application when attempting to reduce the amount of Pb used in perovskite solar modules provided that, as we numerically proved, the use of a h-CPP results in short circuit currents that approach the ones obtained from a standard configuration with approximately half the active layer thickness. For the h-CPP or other periodic types of structuration, a further increase in light absorption would be obtained in the event that structuration on the substrate interface adjacent to the cell would also be implemented, as suggested in Ref. 8 or Ref. 15. In such later cases a periodic distribution of cylinders or prisms on both sides of the substrate was proposed.

6. Experimental section

Preparation of solution precursors: All commercially available chemicals were employed without any further purification. To get the SnO_2 nanoparticle precursor, 134 µL of SnO_2 nanoparticle suspension (Alfa Aesar (tin(IV) oxide, 15% in H_2O colloidal dispersion) were mixed with 866 µL of methanol (Scharlau, 99.5%). Perovskite precursors were prepared inside a N_2 glovebox by dissolving 1.2 M PbI_2 (Sigma Aldrich, 99%) solution in dimethylformamide (Sigma-Aldrich, 99.8%) and dimethylsulfoxide (VWR, 99.5%) with a 4:1 volume ratio and adding 2.5 wt% of $PbBr_2$ (Sigma Aldrich, 99.999%). The solution was kept at 80 ºC and under stirring overnight. The second precursor was prepared by mixing 60 mg of formadinium iodide (Sigma Aldrich, 98%), 6 mg of methylammonium bromide (Sigma Aldrich, 98%) and 6 mg of methylammonium chlorine (Sigma Aldrich) in 1 ml of 2-propanol (Scharlau, 99.5%). A 72.3 mg/ml 2,2',7,7'-Tetrakis[N,N-di(4-methoxyphenyl)amino]-9,9'-spirobifluorene (Spiro-OMeTAD, Merck) solution was prepared in chlorobenzene (Sigma-Aldrich, 99.8%). For the doping of the hole transporting material, 17 µL of a 520 mg/mL bis(trifluoromethylsulfonyl)amine lithium salt(Li-TFSI, Sigma-Aldrich, 99.95%) solution in acetonitrile (Sigma-Aldrich, 99.8%) and 29 µL of 4-tert-butylpyridine (TBP, Sigma-Aldrich 96%) were added to the solution. The polydimethylsiloxane (PDMS, Sylgrad 184, Dow Corning) was prepared in a 8:1 weight ratio of base and curing agents.

Fabrication of perovskite solar cells: Full-covered ITO substrates (100 nm, 15 Ωsq^{-1}, Stuttgart) were employed as substrate for the perovskite solar cell, previously cleaned in 10 minutes cycles of soap solution, water, acetone, water and ethanol. After a UVO treatment of 15 minutes, the SnO_2 nanoparticle solution was spin-coated onto the cleaned ITO substrates at 3500 rpm, followed by a thermal annealing at 150 ºC during 30 minutes in air. The samples were then transferred into a glovebox for next fabrication steps. The lead solution was spin-coated at 60 ºC on top of the electron transporting layer at 2000 rpm. Then, the organic solution was deposited at 2000 rpm for 30 seconds. After some minutes of drying inside the

glovebox, the samples were transferred to a fumehood to perform an annealing at 150 ºC during 20 minutes in ambient air. After that, the Spiro-OMeTAD solution was deposited at 2000 rpm on top of the perovskite layer. The following day, a 60 nm thick gold top contact layer was evaporated in a high vacuum chamber (Lesker). The deposition rate was adjusted to 0.55 Å /s and a metal mask was place to define an active area of 0.096 cm^2.

Thin film characterization: The surface morphology of the h-CPP was evaluated by field emission scanning electron microscopy (FEG-SEM, FEI Inspect F-EBL). Film thickness values were determined employing a surface profilometer (Alpha-Step IQ Surface Profiler, KLA-Tencor) and contrasted by the image obtained of the complete cell cross section with the FEG-SEM. The wavelength-dependent refractive index n and extinction coefficient k of the materials were determined by spectroscopic ellipsometry. For the perovskite, ellipsometric measurements were done with a UV-Vis-NIR Woollam VASE ellipsometer, and analyzed following the same method as in ref 20[22] where n and k were modeled as a sum of Kramers-Kronig consistent oscillators. For the other materials, ellipsometric measurements were done with a UV-Vis-NIR SOPRA GESP5 ellipsometer at angles of incidence between 50º and 70º, and n and k were modeled using a Cauchy law plus Kramers-Kronig consistent oscillators when needed.

Photovoltaic characterization: The photovoltaic performance of the fabricated solar cells was determined using an AM 1.5G solar simulator (Sun 3000, Abet Technologies). The illumination intensity corresponding to 100 $mWcm^{-2}$ was adjusted with a monocrystalline silicon reference cell (Hamamatsu) calibrated at the Fraunhofer Institute for Solar Energy Systems. The current voltage (J-V) curves were then recorded by scanning from positive to negative voltages (1.2 V to -0.1 V) using a Keithley 2400 SourceMeter and a scan speed of 350 mV/s. External quantum efficiency (EQE) analysis was performed using a quantum efficiency measurement system (QEX10, PV Measurements). In this case, the devices were illuminated using a monochromatic light coming from a xenon lamp. The spectral response of

the calibrated silicon cell was used as a reference. All set of devices were tested under ambient conditions.

Supporting Information.
Supporting Information is available from the Wiley Online Library or from the author.

Acknowledgements
This work was supported by the financial support from the Spanish MINECO (Severo Ochoa program, grant No.: SEV-2015-0522), the MINECO and the Fondo Europeo de Desarrollo Regional FEDER (grant No.: MAT2017-89522-R), the Fundació Privada Cellex, the CERCA programme from the Generalitat de Catalunya, and from the EC FP7 Program (ICT-2011.35) under grant agreement n° NMP3-SL-2013-604506. G.K. is a Research Associate with the Belgian Fonds de la Recherche Scientifique-FNRS.

Received:
Revised:
Published online:

REFERENCES

[1] E. Yablonovitch, *J. Opt. Soc. Am.* **1982**, *72*, 899.
[2] A. Mihi, F. J. Beck, T. Lasanta, A. K. Rath, G. Konstantatos, *Adv. Mater.* **2014**, *26*, 443.
[3] R. Hünig, A. Mertens, M. Stephan, A. Schulz, B. Richter, M. Hetterich, M. Powalla, U. Lemmer, A. Colsmann, G. Gomard, *Adv. Opt. Mater.* **2016**, *4*, 1487.
[4] B. Lipovšek, A. Čampa, F. Guo, C. J. Brabec, K. Forberich, K. Janez, M. TopiČ, *Opt. Express* **2017**, *25*, 873.
[5] H. Zhang, M. Kramarenko, J. Osmond, J. Toudert, J. Martorell, *ACS Photonics* **2018**, *5*, 2243.
[6] L. Zheng, Y. Ma, S. Chu, S. Wang, B. Qu, L. Xiao, Z. Chen, Q. Gong, Z. Wu, X. Hou, *Nanoscale* **2014**, *6*, 8171.
[7] D. Liu, T. L. Kelly, *Nat. Photonics* **2014**, *8*, 133.
[8] M. Mariano, G. Kozyreff, L. G. Gerling, P. Romero-Gomez, J. Puigdollers, J. Bravo-Abad, J. Martorell, *Light Sci. Appl.* **2016**, *5*, e16216.
[9] W. S. Yang, B.-W. Park, E. H. Jung, N. J. Jeon, Y. C. Kim, D. U. Lee, S. S. Shin, J. Seo, E. K. Kim, J. H. Noh, S. Il Seok, *Science (80-.).* **2017**, *356*, 1376.
[10] Q. Jiang, L. Zhang, H. Wang, X. Yang, J. Meng, H. Liu, Z. Yin, J. Wu, X. Zhang, J. You, *Nat. Energy* **2016**, *2*, 16177.
[11] M. M. Tavakoli, K.-H. Tsui, Q. Zhang, J. He, Y. Yao, D. Li, Z. Fan, *ACS Nano* **2015**, *9*, 10287.
[12] B. Dudem, J. H. Heo, J. W. Leem, J. S. Yu, S. H. Im, *J. Mater. Chem. A* **2016**, *4*, 7573.
[13] M. Jošt, S. Albrecht, L. Kegelmann, C. M. Wolff, F. Lang, B. Lipovšek, J. Krč, L. Korte, D. Neher, B. Rech, M. Topič, *ACS Photonics* **2017**, *4*, 1232.
[14] J. Wei, R. P. Xu, Y. Q. Li, C. Li, J. De Chen, X. D. Zhao, Z. Z. Xie, C. S. Lee, W. J. Zhang, J. X. Tang, *Adv. Energy Mater.* **2017**, *7*, 1.
[15] Y. Li, T. Jiang, X. He, Y. Zhang, C. Fang, Z. Li, J. Lin, Y. Zhuang, *Opt. Commun.* **2019**, *439*, 118.
[16] D.-L. Wang, H.-J. Cui, G.-J. Hou, Z.-G. Zhu, Q.-B. Yan, G. Su, *Sci. Rep.* **2016**, *6*, 18922.
[17] R. T. Ginting, E. B. Jeon, J. M. Kim, W. Y. Jin, J. W. Kang, *ACS Appl. Mater.*

Interfaces **2018**, *10*, 31291.
[18] N. J. Jeon, J. H. Noh, W. S. Yang, Y. C. Kim, S. Ryu, J. Seo, S. Il Seok, *Nature* **2015**, *517*, 476.
[19] N. Pellet, P. Gao, G. Gregori, T. Y. Yang, M. K. Nazeeruddin, J. Maier, M. Gr??tzel, *Angew. Chemie - Int. Ed.* **2014**, *53*, 3151.
[20] M. A. Kats, R. Blanchard, P. Genevet, F. Capasso, *Nat. Mater.* **2013**, *12*, 20.
[21] M. A. Kats, R. Blanchard, S. Ramanathan, F. Capasoo, *Opt. Photonics News* **2014**, *25*, 40.
[22] Q. Liu, P. Romero-gomez, P. Mantilla-perez, S. Colodrero, J. Toudert, J. Martorell, *Adv. Energy Mater.* **2017**, *7*, 1700356.

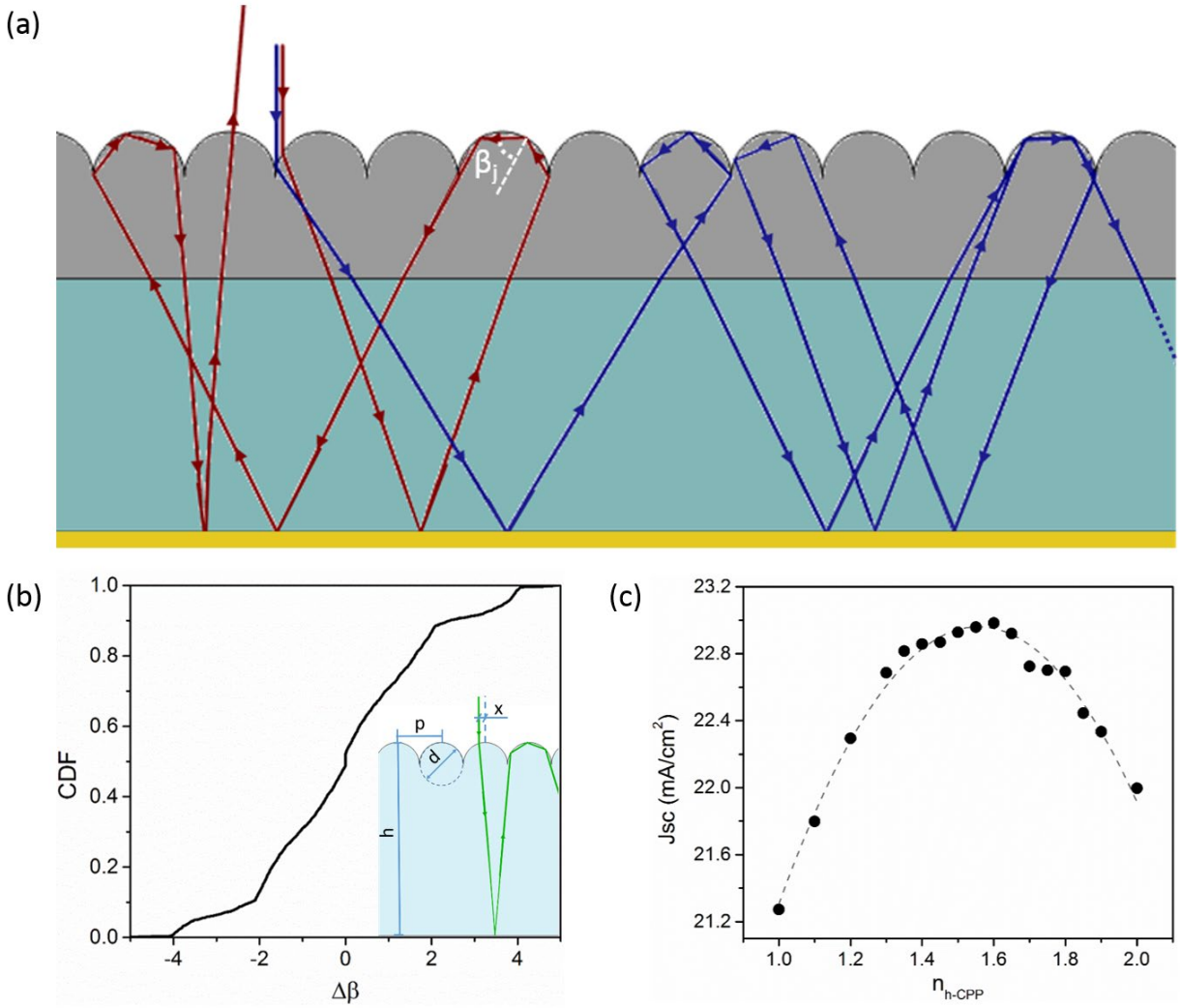

Figure 1. (a) Ray trajectory simulation of two different rays upon an h-CPP on glass. (b) CDF related to the Δβ computed over a series of ray segments. (c) Short circuit current (solid dots) as a function of the index of refraction for the h-CPP/substrate structure. In this numerical computation we assumed the index of refraction of the h-CPP and substrate are the same. The dotted line is a guidance of the eye.

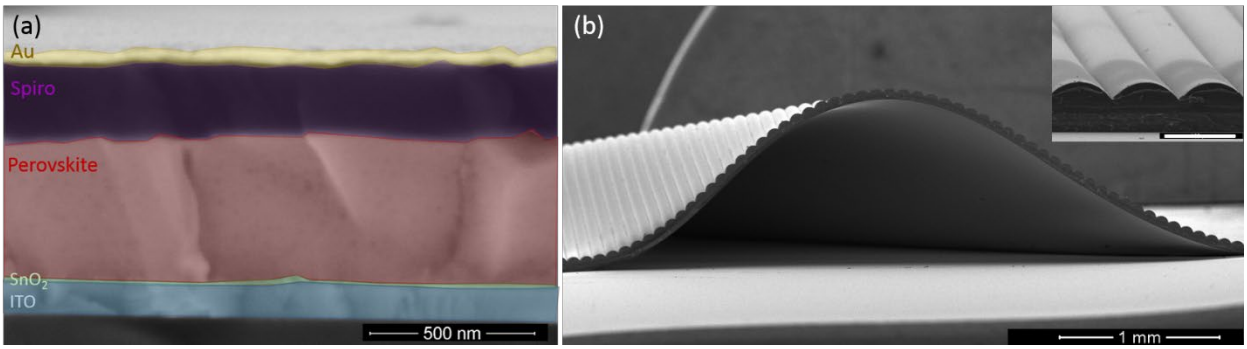

Figure 2. (a) Cross section SEM image of a perovskite solar cell. The layers have been tinted to identify them clearly. (b) Cross section SEM image of a free standing h-CPP. The inset represents a closer view of the h-CPP, the scale bar in the inset corresponds to 100 μm.

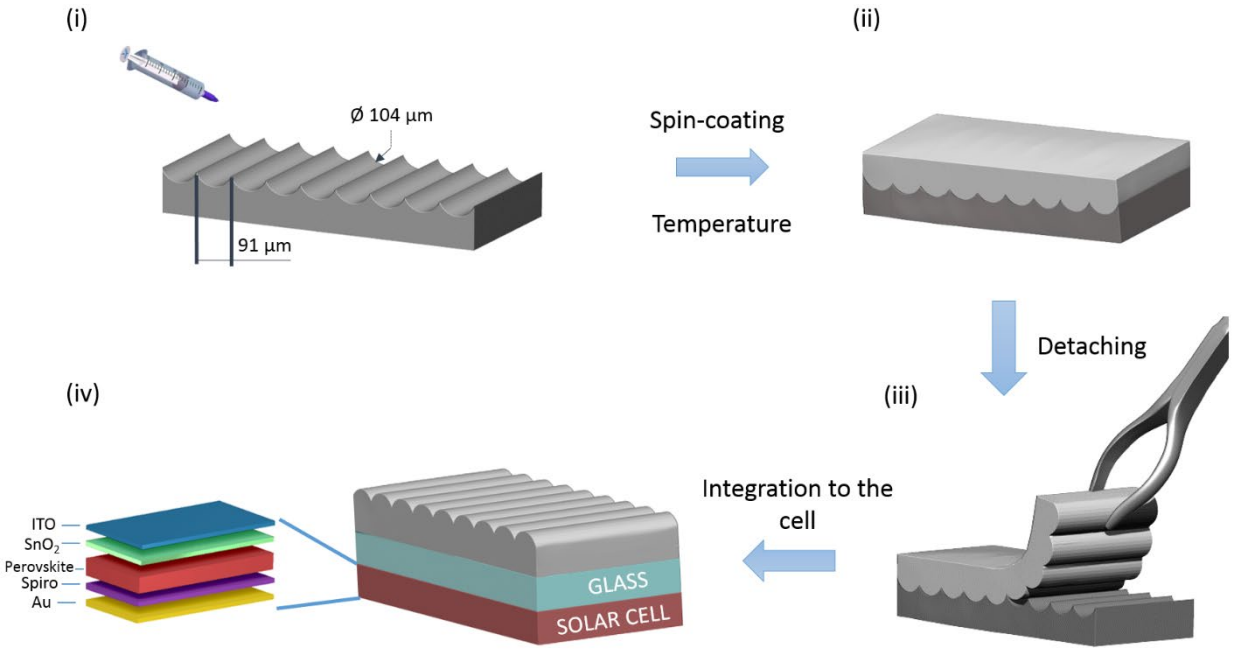

Scheme 1. h-CPP fabrication process: (i) Deposition of the PDMS on the master. (ii) After spin-coating and annealing of the film the PDMS is cured. (iii) Then, the PDMS is detached from the master obtaining the h-CPP. (iv) The h-CPP is integrated to the solar cell by attaching it to the glass side.

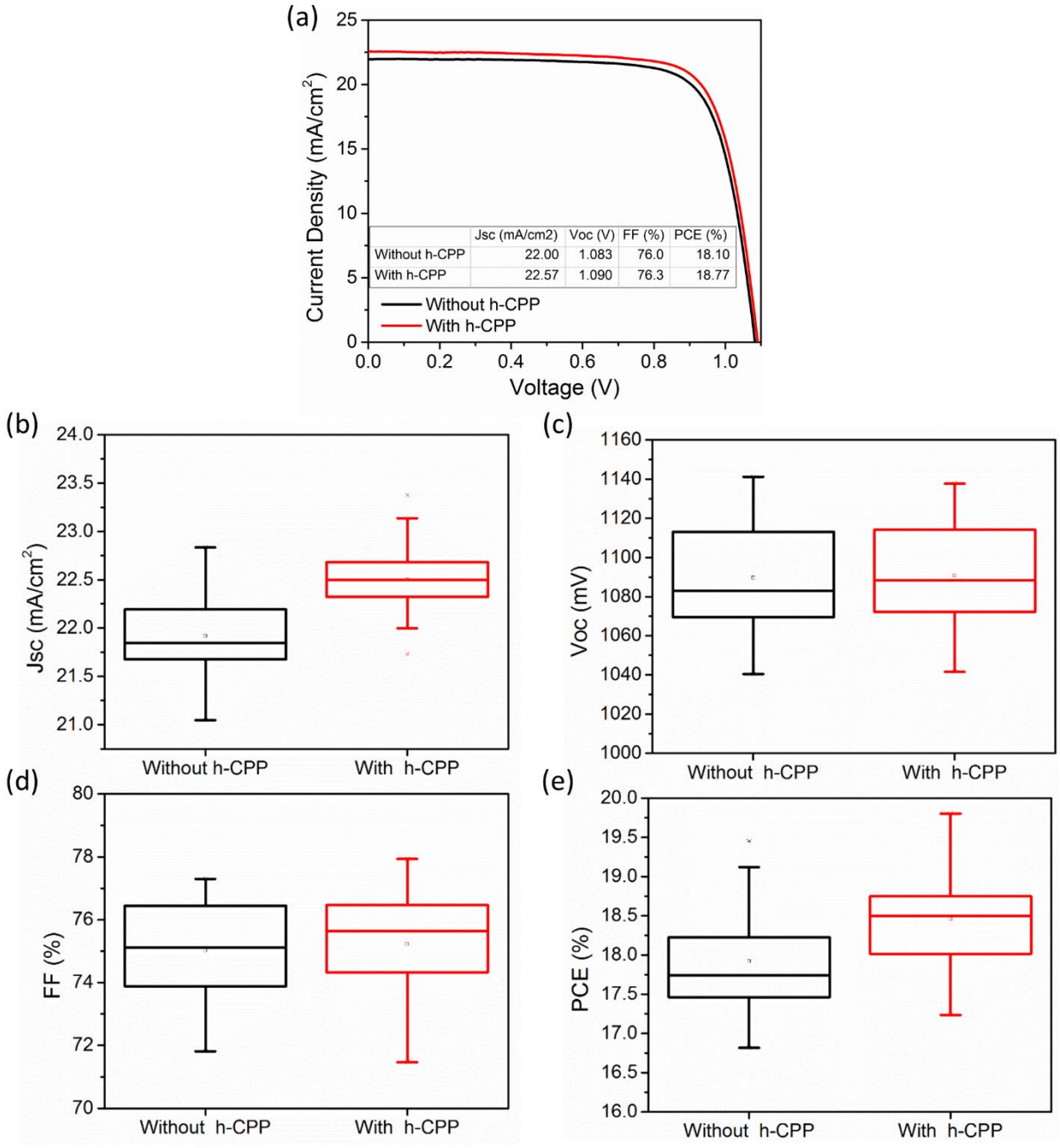

Figure 3. (a) J-V curves of a representative device with and without h-CPP. (b) Jsc, (c) Voc, (d) FF and (e) PCE statistical analysis of 24 different perovskite solar cells with and without the h-CPP.

Table 1. Average photovoltaic parameters and gain obtained for 24 devices with and without the h-CPP.

	Jsc [mA/cm^2]	Voc [V]	FF [%]	PCE [%]	Best PCE [%]
Without h-CPP	21.81 ± 0.53	1.088 ± 0.03	75.07 ± 1.5	17.82 ± 0.72	19.44
With h-CPP	22.39 ± 0.54	1.089 ± 0.03	75.28 ± 1.8	18.36 ± 0.74	19.81
Gain	0.58 ± 0.12	0.001 ± 0.006	0.21 ± 0.67	0.54 ± 0.19	

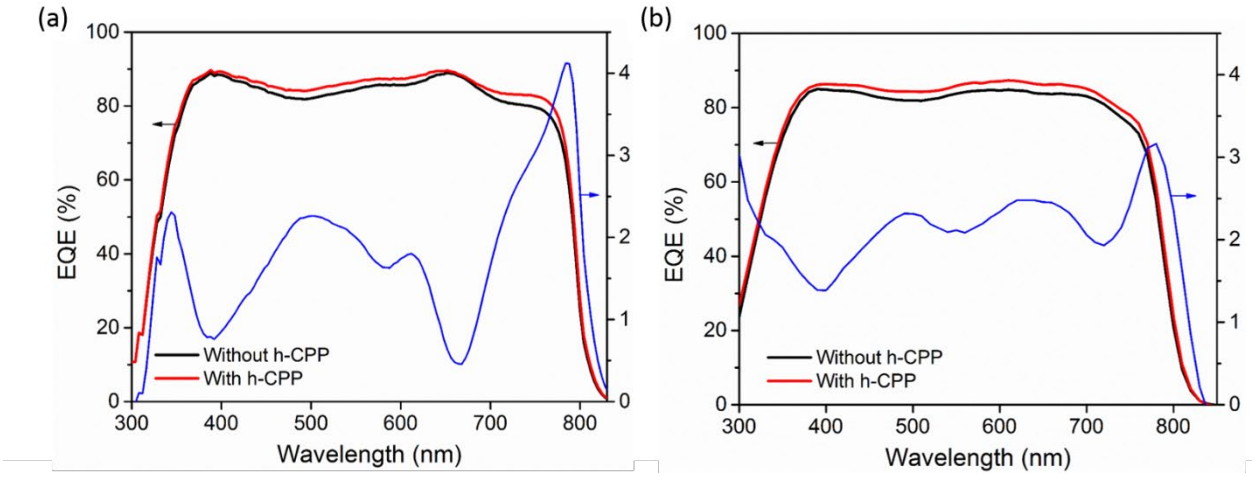

Figure 4. (a) Simulated and (b) experimental EQE for solar cells with (red curve) and without h-CPP (black curve). Blue curves represent the EQE gain depending on the wavelength.

We designed a periodic half-cylinder photonic plate to achieve a 97% randomization in the light propagation. When such ergodic light propagation is applied to increase the absorption path length in a planar geometry perovskite solar cell, we demonstrate that we can to obtain the maximum possible short circuit current enhancement provided by light randomization.

Ergodic light propagation

Guillermo Martínez-Denegri*, Silvia Colodrero, Quan Liu, Johann Toudert, Gregory Koyreff, and Jordi Martorell*

Ergodic light propagation in a half-cylinder photonic plate for optimal absorption in perovskite solar cells

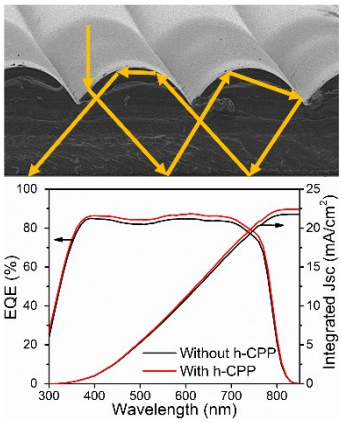

Supporting Information

Ergodic light propagation in a half-cylinder photonic plate for optimal absorption in perovskite solar cells

Guillermo Martínez-Denegri, Silvia Colodrero, Quan Liu, Johann Toudert, Gregory Kozyreff, and Jordi Martorell**

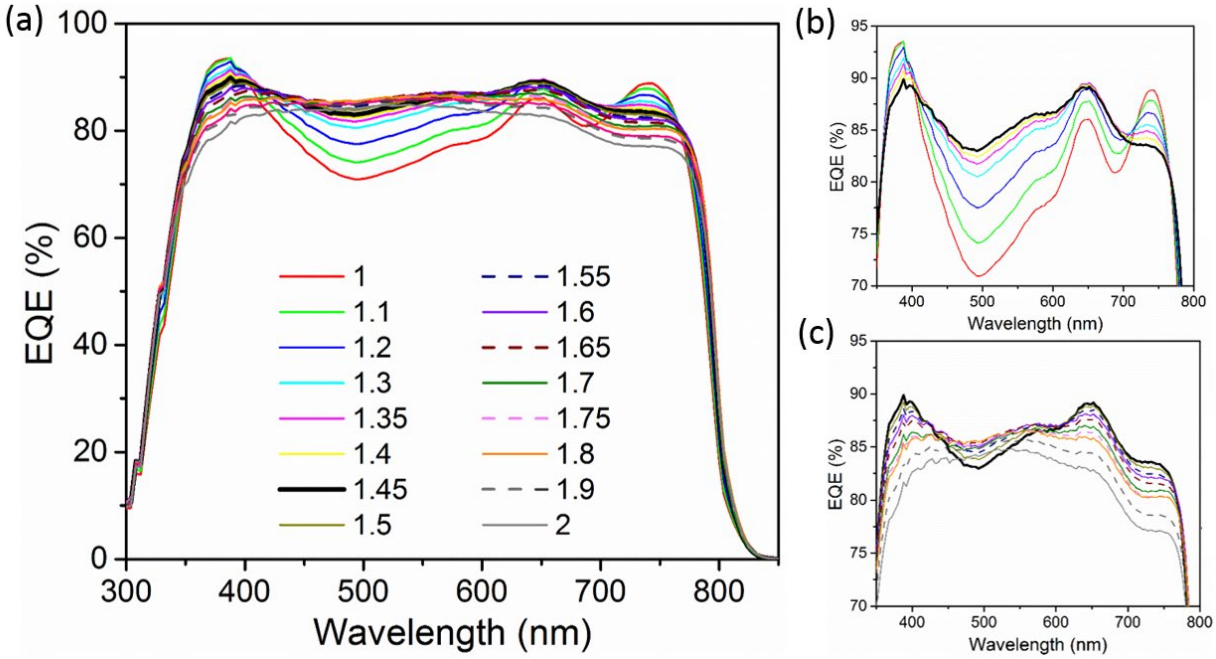

Figure S1. (a) Simulated EQE for devices with h-CPP considering different h-CPP refractive index. (b) Zoom in of the EQE curves for n ≤ 1.45. (c) Zoom in of the EQE curves for n ≥ 1.45.

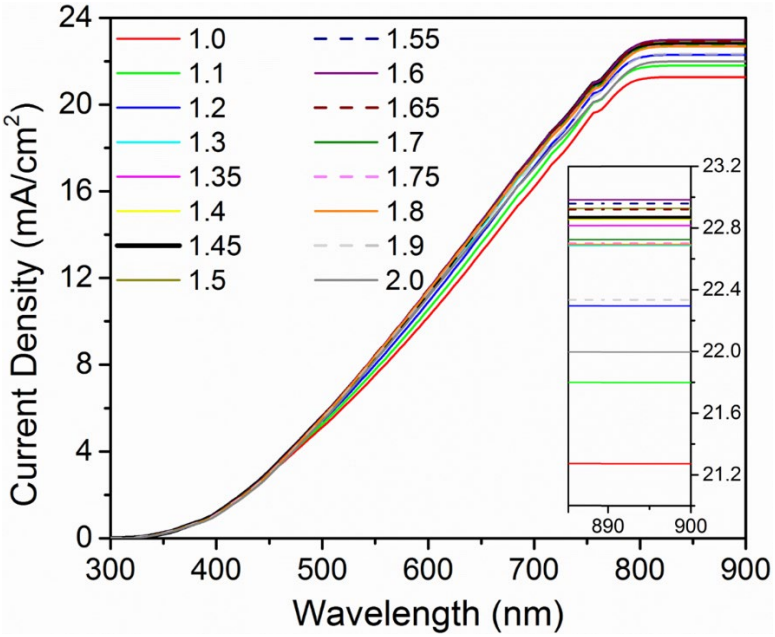

Figure S2. Simulated Jsc obtained from integrating the EQE results for a device with h-CPP considering different h-CPP refractive index. The inset represents an amplification of the final wavelength area.

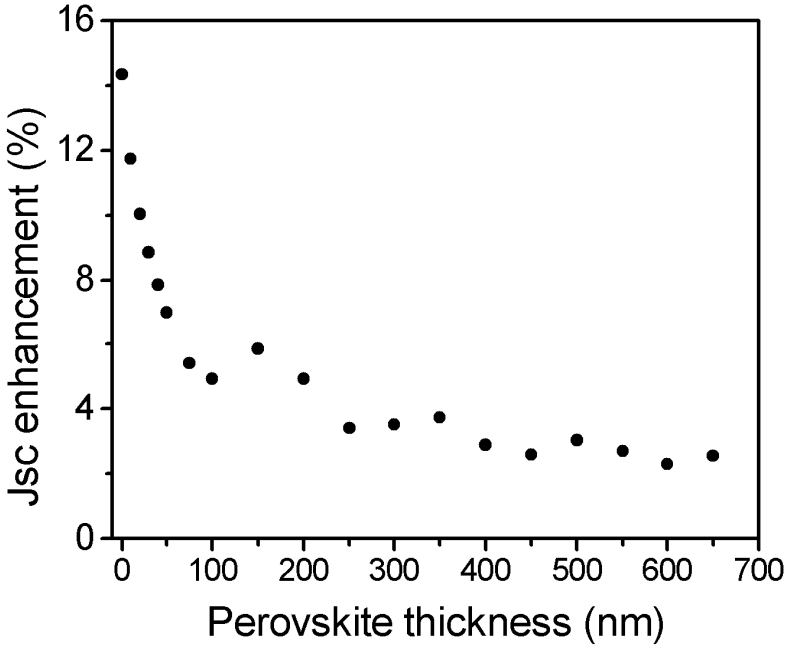

Figure S3. Simulated Jsc enhancement when the h-CPP structure is added for different perovskite thickness solar cells.

The graph shows how the Jsc enhancement declines as the perovskite layer thickness decreases. From this analysis, one may conclude that when the perovskite layer is thick

enough, since ergodicity will not have a detrimental effect in light absorption, the Jsc enhancement will converge to a value comparable to the gain obtained by using a simple antireflective coating.

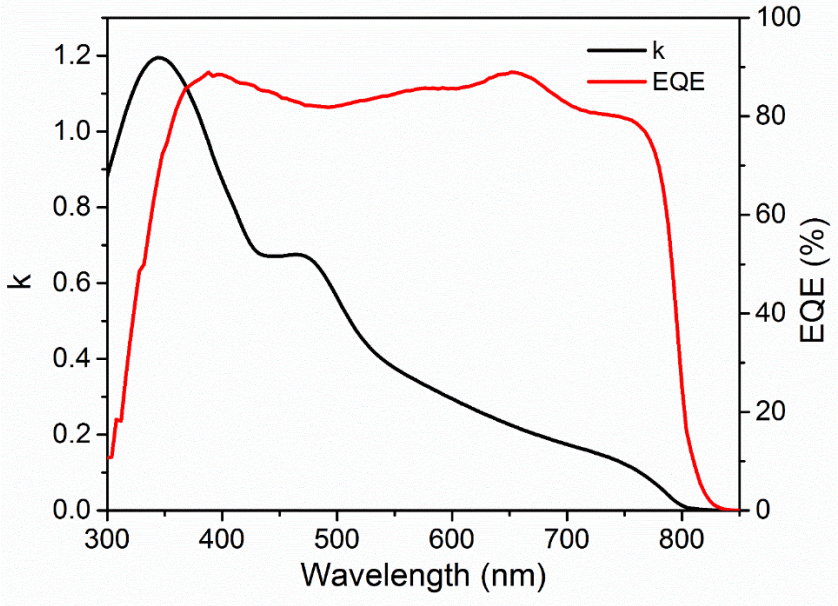

Figure S4. Comparison between the simulated EQE curve for a planar device and its perovskite extinction coefficient (k).